Proceedings of the Canadian Society for Mechanical Engineering International Congress 2021
CSME Congress 2021
June 27-30, 2021, Charlottetown, PE, Canada

An Innovative Model Temperature Prediction for a Pulley in a Belt Drive

Xingchen Liu[1], Kamran Behdinan[1*]
[1] Department of Mechanical & Industrial Engineering, University of Toronto, Toronto, Canada
*behdinan@mie.utoronto.ca

Abstract—This paper includes developing a thermal model that can predict the instant thermal distribution of fibre-reinforced polymers (FRPs) pulley within a belt drive. The use of FRPs has increased the possibility of thermal destruction. Therefore, this work presents an innovative and advanced model for efficiently and accurately calculate temperature distributions. It uses the classical heat partitioning equations and then the novel analytical-numerical method to calculate the thermal distribution. Validations were conducted and demonstrated good agreement with the calculated temperatures. The deviations are below 20% of absolute temperature rise and the solution time is less than ten seconds.

Keywords-component; Belt drive; Thermal measurement; Thermal analysis; Vehicle engine

I. INTRODUCTION

The belt drive is a transmission system used in the automobile industry. The power is transmitted from the engine crankshaft to individual auxiliary components. Hence, it is a critical system inside the engine that ensures the reliability of the overall engine power output [1]. Presently, a growing number of pulleys are fabricated from advanced materials called fibre-reinforced polymers (FRPs), replacing traditional steel [2]. Although FRPs are robust, light-weight and cost-effective composite, they have a low thermal conductivity that requires extra consideration of their thermal behaviours [3], [4]. A belt system dissipates energy during the operation, together with the hot conditions of the under-the-hood engine environment, the resulting temperature can lead to an increased probability of thermal deterioration failure [5]. The primary explanation for this is that the excessive accumulated heat cannot dissipate into the environment, resulting in deterioration and blistering [6]. Therefore, it is necessary to develop an innovative thermal analytical model that can rapidly calculate the heat distribution of a pulley under various operating conditions, allowing for the avoidance of thermal destruction and prolonging the product life [7].

The thermal calculations consist of two primary sub-calculations. The first confirms the heat generation and the second analyzes the heat transfer behaviours.

Heat sources and their locations are highly associated with power loss because all lost energy is transformed into heat. The classic and most predominant power loss theory considers power loss stem from five sources: belt shear, radial compression, bending, tension and pulley–belt frictional slip [8]. The first four losses occur due to belt hysteresis deformations inside the belt, while slip loss is the result of belt-pulley frictional slippage. This theory was later enhanced by Manin [9] for application in poly-V belt drive systems. Silva [10], [11] considered that the sources of power loss to be from belt rubber hysteresis because of dynamic stretching, bending, flank, shear and circular compression of the belt material.

Heat analyses for the belt drives have been researched. One study used Jaeger's classical heat source method to establish general analytical solutions for temperature increases related to various forms of contact surfaces and thermal intensity distribution [12]. Some three-dimensional analytical models were created both theoretically and experimentally to predict contact surface temperatures and heat partitioning coefficients for cylinderical scenarios [13][14]. Another study established an analytical-numerical algorithm to calculate the heat map of an entire braking system with the disk and pad inside [15].

Currently, only a handful of investigations have attempted to speed up the thermal evaluation. This research thus develops a thermal model that can effectively predict the heat distribution of a pulley at numerous operating conditions. Moreover, an experiment has been performed under a variety of engine conditions to prove the resultant validity.

II. FUNDAMENTAL MODELLING

The purpose of this thermal model is to provide heat information of an individual pulley inside the belt drive system, ensuring that this pulley is at the safe operating temperature. The goal of this work is to provide instant temperature results and without a decrease in accuracy.

This model consists of three sub-sections in this study. Figure 1 displays the workflow of the model. The first section explains the calculation of thermal generation inside the belt drive. The second section discusses the adoption of the band contact algorithm [16] to determine the partitioning of frictional heat at the pulley–belt surfaces and calculates the fraction of generated frictional heat transferring into the pulley P_f. This model uses ξ as the heat partition coefficient to denote the percentage of frictional heat transferring to the pulley. The

last section develops analytical-numerical thermal analysis, considering the complex pulley geometries and turbulent flow around the pulley, to deliver the instant heat map of the pulley under designed operating condition.

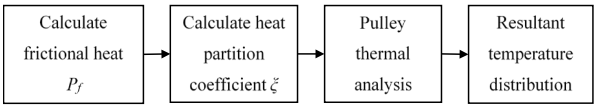

Figure 1. Single pulley model.

A. Thermal Generation within the System

The first step is to calculate the heat generation and locations inside the drive system through the operation. Transmission energy loss theory can be utilized as the heat generation calculation. This study uses a prevalent classical power loss theory, classifying the heat flux generated according to their locations [17]. There are two groups of power losses that occur inside a system. The first group is the internal energy loss of the belt P_h, which is generated at different sections of the belt. It consists of four different hysteresis power losses caused by bending, stretching, tension, and shear radial compression. The next group is the contact surface power loss P_{fn}, which is generated at the pulley–belt engaged surface. This heat is due to the frictional belt–pulley slip.

However, P_f is considered the only heat source in this thermal model because P_f is the primary source, which accounts for 70% to 80% of the total heat generation. The calculation of P_f is achieved through the belt pressure distribution on surfaces in contact with the pulley and the frictional distance in unit time [18]:

$$P_f = \int_0^{\alpha} \mu p(\alpha) v d\varphi \tag{1}$$

where μ is the coefficient of frictional (COF); p is the pressure distribution the belt applies on the pulley; v is the relative engaged surface speed; α is the angle in degrees; and $d\varphi$ is an infinitesimal angular element of α.

B. Calculation of Heat Partitioning Coefficient

The second step is to ascertain the proportion of P_f calculated from the prior step that transfers to the pulley. This calculation is important for the pulley thermal analysis conducted in the third step. Frictional heat generally flows to both sides of the contacted surface, which in this case are the pulley and belt. There is a percentage of frictional heat (denoted as ξ) flowing to the pulley. This model introduces a band contact algorithm from the pad-on-disk application to calculate the ξ. The relative sliding between the belt and pulley during operation can be considered as the pulley rotating against the stationary belt at a relative speed v. Thus, the calculation for the heat partitioning coefficient in that situation [19] can be applied:

$$\xi = 1 - 1/\left(1 + \Lambda_b / \Lambda_p * \sqrt{1 + Pe}\right) \tag{2}$$

where the thermal conductivities of the belt and pulley are Λ_b and Λ_p, respectively; the Péclet number is calculated as $Pe = vW_b / 2\kappa_b$; the belt width W_b is 0.0024 m; κ_b is the the belt's thermal diffusivity, which is 0.12 m^2/s. The maximum belt speed is 35.6 m/s, and the slip rate varies from 0.5% to 2.5% during operation. This makes the Pe approximate to 0. Therefore, Φ_p, the amount of heat flowing into the pulley per second, can be calculated as:

$$\Phi_p = \Lambda_p P_f / (\Lambda_p + \Lambda_b) \tag{3}$$

All of the heat coming from the outside [20] and entering into the pulley eventually disperses into the environment. Therefore, Φ_p from Equation (3) is also equal to the heat dissipation rate from all the pulley's exposed surfaces.

C. Calculation of Heat Partitioning Coefficient

The third step is to use the value for Φ_p to determine the heat plot of the pulley under the design cycles. The benefit of adopting the numerical method is to consider the complicated geometries and turbulence. To calculate the temperature immediately, this study introduces λ_p to represent the ratio of Φ_p and T_{pc}. This value can be affected by a lot of operating parameters. However, the structure of the pulley remains unchanged during the operation. One research provided that the ambient temperature and COF do not affect the λ_p [21]. Another research indicated that the contacted temperature with the belt has no effect on the ratio of Φ_p and T_{pc}. And the rotation speed has a nonlinear relationship on this ratio[22]. Therefore, $S(\omega_p)$ is used for the curve of λ_p and ω_p. The target of this numerical simulation is to create a set of values { $S(\omega_p)$, $\mathbf{T}_p^{'}$, $\Phi_p^{'}$ } is established for the pulley spinning at baseline speeds in growths of 1000 RPM. $\mathbf{T}_p^{'}$ and $\Phi_p^{'}$ are under baseline conditions and prime are added. They are collected for following pulley heat distribution calculations [14].

1) Modelling Structure

This CFD model contains both solid and fluid regions. The solid region represents the pulley and shaft. Conversely, the fluid region is used to simulate airflow surrounding the solid region. Its diameter is four times greater than the maximum diameter of the pulley, offering an adequately substantial space to calculate turbulence flow. The belt is suppressed because its thin shape does not significantly influence the temperature distribution of the pulley.

2) Modelling Motions

This simulation uses the single reference frame (SRF) technique to simulate the relative motion between the components and surrounding air. The study sets the fluid domain rotating against the stable solid domain to replicate the high-speed spinning pulley rotating against the air. Only turbulence flow and heat transfer are simulated inside the fluid domain and heat transfer within the solid domain. The complexity of this calculation is then reduced to a static-state

analysis from a fluid-structure interaction, by this means increasing the computational speed.

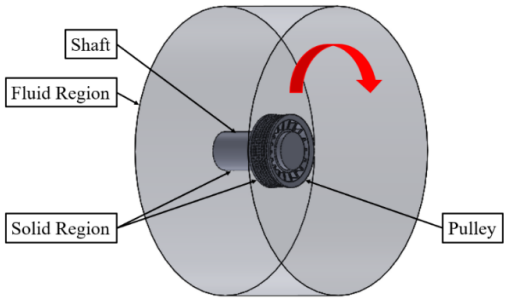

Figure 2. CAD model used for the simulation.

3) Meshing Procedure

The same mesh technique is applied to both the solid and fluid regions. This simulation generates the triangular surface mesh and transforms it into polyhedrons in order to decrease the number of cells. The mesh is set to fine around the contact surfaces and steadily turns out to be coarser as it is close to the inner radius of the pulley, as shown in Figure 3. Additionally, this simulation sets the conformal meshes at the interfaces of each connected region to ensure that they use the same element edges and nodes at the interfaces, accelerating the calculation by enhancing the convergence rate and computational stability.

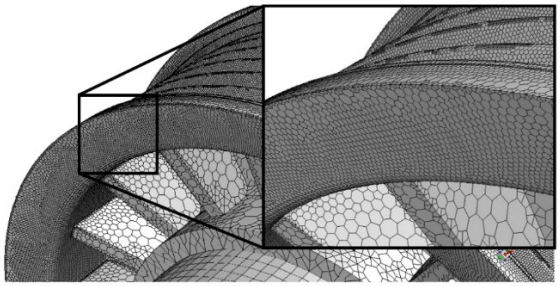

Figure 3. Polyhedral mesh for the numerical analysis.

4) Modelling Heat Transfer

Creating the modelling for the heat analysis is challenging because this establishing needs a precise turbulence model to mimic the flow of air induced by the high-speed rotation of the pulley and an accurate method to compute the heat dissipation rate on the exposed surfaces under such an airflow. The SST k–ω model includes the pressure-based solver and uses the incompressible ideal gas equation for the air density within the fluid region. This model can be used to simulate the turbulence flow caused by the motions of the fins and calculate the heat dissipation based on the local airspeed achieved by the SST near-wall treatment. Furthermore, the ambient temperature is used as the initial temperature. The ISO 22007-2 is used to measure the thermal conductivity for FRP for high accurate simulation.

5) Input/Output Setting

Special treatment for the definition of thermal flux Φ_p is required in this simulation. During the pulley's operation, when the red surfaces of the grooved feature highlighted in Figure 4.1 come in contact with the belt-engaged surfaces, friction happens and generates heat. A percentage of that heat enters the pulley, and the heat flow direction of these surfaces point inward to the pulley. When the pulley disengages with the belt after rotating a certain degree, heat is dissipated from those red surfaces into the environment. The heat flow direction of these surfaces points outward to the pulley. It is impossible for a static numerical simulation to define the flow direction changes. Consequently, this study allocates small solid sections adjacent to the red surfaces (highlighted in blue in Figure 4) to simulate the frictional heat generation. The red surfaces are defined as the heat always dissipates to the fluid domain.

The zero-gauge pressure is set at the pressure outlet boundary of the fluid domain. The end surface of the shaft is set to a constant ambient temperature. The default setting of the backflow's turbulent intensity and viscosity are used.

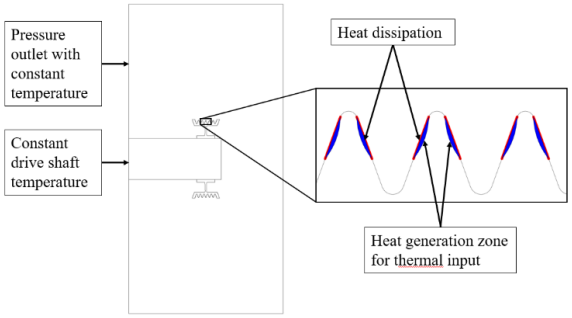

Figure 4. Boundary conditions for the numerical analysis.

The resultant simulations from the numerical approach provide valuable information, including the temperature distribution of the pulley $\mathbf{T}_p^{'}$, the average area-weight temperature at the contact surfaces of pulley $T_{pc}^{'}$ and $\Phi_p^{'}$.

6) Parametric Setting

The target of this numerical simulation $S(\omega_p)$ is calculated by a parametric study. In this analysis, the ω_p has incremental intervals of 1000 RPM. In every interval of ω_p, the input into the numerical model is the heat generation, and the output has $\Phi_p^{''}$ and $T_{pc}^{''}$. Thus, a database is established for all the pulleys at available range of speed.

D. Calculation of Heat Partitioning Coefficient

The value of $\Phi_p^{''}$ and $\mathbf{T}_p^{''}$ at the design speed ω_p can be acquired using the linear interpolation. Next, the temperature distribution of the pulley is calculated by Equation (4).

$$\mathbf{T}_p = \Phi_p / \Phi_p^{''} \left(\mathbf{T}_p^{''} - T_a \right) + T_a \tag{4}$$

Identify applicable sponsor/s here. *(sponsors)*

III. EXPERIMENTAL SETUP

This experiment plans to experimentally prove the model's resultant temperature results, proving this model's high reliability. The validation processes measure the surface temperatures of this drive system and evaluate them with the related predicted temperature results from the thermal model at a variety of scenarios.

A. Load Case

The validation of this drive system under certain operating conditions is vital to proving the reliability of the thermal models, like other works [23]. To cover these variations in pulley parameters, this experiment uses different pulley radii, output transmitted speed, slip rate. Table 1 presents the list of parameters covering the range of engine operating conditions.

TABLE I. OPERATING CONDITIONS

Parameter	Variation
Pulley Radius (mm)	62 / 85 / 108
Transmitted Speed (RPM)	2000 – 7000
Slip Rate	Half / Full

B. Layout Setup

One belt drive layout was designed and used in this experiment, with the following considerations. The first factor is the interchangeability of the pulleys to test the various radii. The second factor is the stability of the belt drive system. This belt layout contains three extra pulleys beyond the DN and DR pulleys. One pulley measures belt tension, while another measures belt speed. The third pulley is connected to the belt tensioner, which reduces the belt vibration. The last consideration involves leaving space for the infrared sensors. The measured dimensions of each sensor and its focus distances were taken into account.

C. Installation

The last step of the experiment setup is to install the belt drive system on this modified engine dynamometer, as shown in Figure 5 [24]. The customized insulated chamber is fabricated and mounted on the dynamometer. Foam is mounted on the wall to provide better heat insulation. There are five infrared sensors targeting the different surfaces to acquire local temperatures. An extra thermal imaging camera functioning as a second measurement system is focused on the DN pulley to capture the temperature distribution. All temperature information is transmitted from sensors to a data acquisition system.

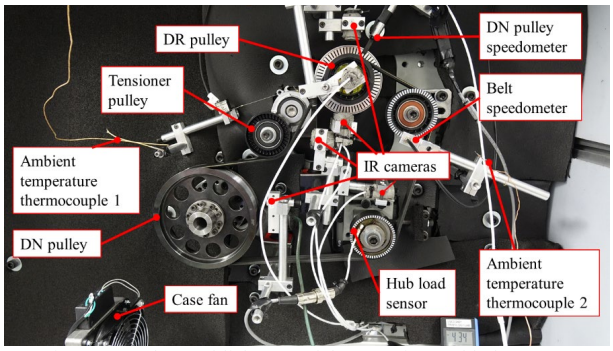

Figure 1. The establishment of the experimental belt system.

IV. RESULT AND DISCUSSIONS

To show the reliability and precision of these three models, the calculated and experimental temperatures obtained under a variety of pulley radii, slip rate, and speeds, as described in Table 1, are investigated below.

A. Radius Influence

The first step is to examine the impact of the pulley radius on heat distribution. Figure 6 reveals the calculated and experimental temperatures at the outer edges of FRP pulleys with different radii rotating at 3,000 RPM. Most importantly, these calculated results show excellent agreement with the experimental ones. The maximum variation is 2℃, which is below 20% of the total temperature rise, meeting the accuracy requirement.

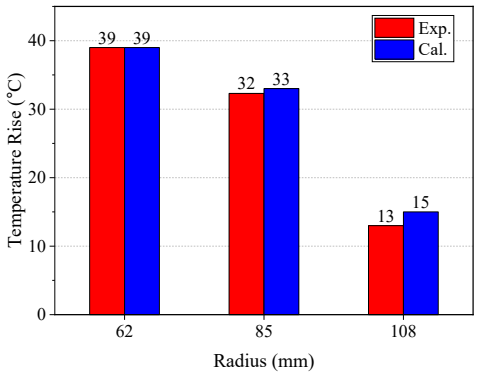

Figure 1. Comparison of experimental and calculated temperatures at the outer edges of different radii of three pulleys under the half-slip operating condition and constant spinning speed of 3,000 RPM.

B. Torque Influence

Enhanced belt slip causes greater frictional heat and higher peak temperatures at the outside radius of a pulley. This comparison applied various torque loads on DN pulleys and got several slip rates. Figures 7 (a) and (b) display the experimental and calculated temperatures at the outer radii of two pulleys at half- and full-slip conditions. The calculated temperatures show the same trends as those observed in the measurements. The largest difference is 3℃, and all the differences are below 20% of the total temperature rise.

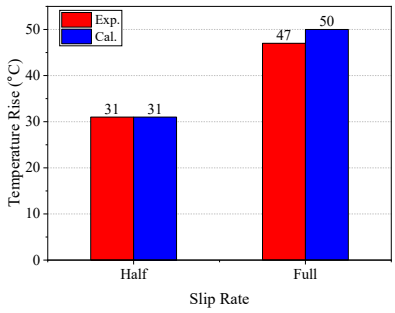

(a)

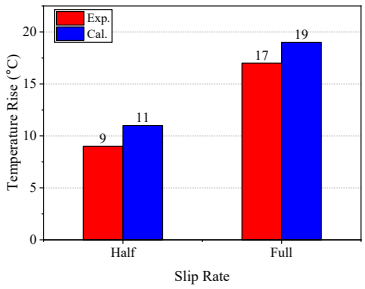

(b)

Figure 2. Comparisons of the experimental and calculated temperatures on the surfaces at the outside radii of two pulleys at 2,000 RPM and half- and full-slip operating conditions for (a) 62 mm and (b) 108 mm pulleys.

C. *Rotation Influence*

Pulley rotation speed is another factor influencing the temperature distribution of a pulley. The moves in speed change not only heat dissipation at exposed surfaces but also frictional heat production. Figure 8 displays the temperatures calculated on the surface at the outside edges of a pulley with a radius of 108 mm running from 2,000 to 7,000 RPM. The maximum difference is 8℃; however, this is still acceptable when the maximum allowable variation is 20% of the total temperature rise.

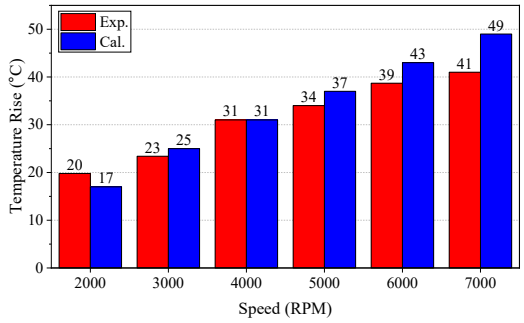

Figure 8. Comparisons between experimental (Exp) and calculated (Cal) temperatures for the pulley with 108 mm at speeds from 2000 to 7000 rpm and the half-slip condition.

D. *Pulley Temperature Profile Influence*

Additional evaluation of this thermal model is the pulley heat distribution. The mid-web of pulley has the most radial distance. This comparison focuses on this section along the outer surface of the pulley. Figures 9 (a) and (b) show the calculated temperature distributions at different points along the radial direction for 62 mm and 108 mm pulleys. The calculated thermal lines are matching the measured temperatures at five different locations. The largest difference is less than 4˚C. Therefore, it proves that this model could effectively calculate the temperature gradient along the radial direction.

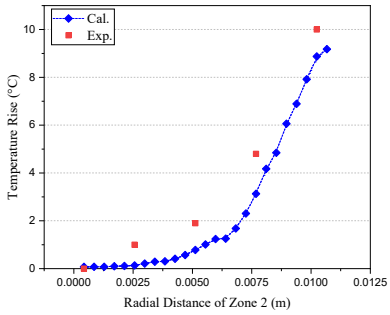

(a)

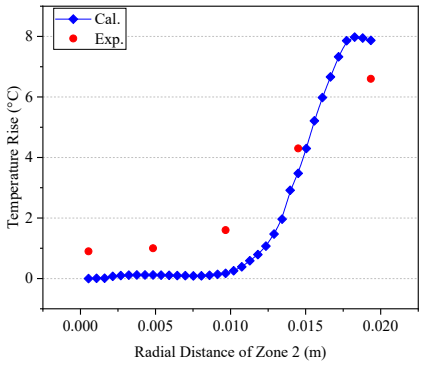

(b)

Figure 3. Evaluations of the experimental (Exp.) and calculated (Calc.) heat gradients of mid webs on two pulleys under the 6,000 RPM and half-slip operating condition: (a) 62 mm and (b) 108 mm diameters.

V. CONCLUSION

This paper introduces the thermal model to calculate heat distributions of a pulley inside the belt drive in an efficient and precise manner. The significant achievement this research is the computation of the surface temperature distribution instantly. The most important creation of this approach is using the classical heat partitioning theory, together with an analytical-numerical method to calculate heat distribution inside a pulley. Moreover, this study includes the experiments at a variety of operating conditions and validations between the calculated and experimental results. The resultant calculated temperatures are in good agreement with the experimental values, demonstrating the high precision and consistency of these models. Overall, this model can effectively compute the heat distribution of a pulley within a belt transmission under a variety of operating conditions within less than 10 seconds (without the time spent on establishing the numerical database for the baseline conditions, which must be done in advance).

ACKNOWLEDGMENT

Funding for this research was obtained from ARL-MLS lab and Litens Automotive Group, and is gratefully acknowledged.

REFERENCES

[1] G. Song, K. Chandrashekhara, W. F. Breig, D. L. Klein, and L. R. Oliver, "Failure analysis of serpentine V-ribbed belt drive system," in *SAE Technical Papers*, 2004.

[2] R. Ufuk and M. Ereke, "Composite material optimization for heavy duty chassis by finite element analysis," *Adv. Automot. Eng.*, vol. 1, no. 1, pp. 41–59, 2018.

[3] M. Gadalla and H. El Kadi, "Evaluation of thermal stability of quasi-isotropic composite/polymeric cylindrical structures under extreme climatic conditions," *Struct. Eng. Mech.*, vol. 32, no. 3, pp. 429–445, Jun. 2009.

[4] S. H. Kim, Y. J. Heo, and S. J. Park, "Ozonization of SWCNTs on thermal/mechanical properties of basalt fiber-reinforced composites," *Steel Compos. Struct.*, vol. 31, no. 5, pp. 517–527, Jun. 2019.

[5] S. Kim, J. Shim, J. Y. Rhee, D. Jung, and C. Park, "Temperature Distribution Characteristics of Concrete during Fire Occurrence in a Tunnel," *Appl. Sci.*, vol. 9, no. 22, p. 4740, Nov. 2019.

[6] H. Oka, Y. Tabuchi, and H. Yazawa, "Development of Plastic Pulley for Automotive Air Conditioner Compressor," in *SAE Technical Paper Series*, 2002, vol. 111, pp. 2002–2008.

[7] P. Guan, Y. Ai, C. Fei, and Y. Yao, "Thermal Fatigue Life Prediction of Thermal Barrier Coat on Nozzle Guide Vane via Master–Slave Model," *Appl. Sci.*, vol. 9, no. 20, p. 4357, Oct. 2019.

[8] B. G. Gerbert, "Power Loss and Optimum Tensioning of V-Belt Drives," *J. Eng. Ind.*, vol. 96, no. 3, p. 877, Aug. 1974.

[9] L. Manin, X. Liang, and C. Lorenzon, "Power losses prediction in poly-v belt transmissions: application to front engine accessory drives," in *International Gear Conference 2014: 26th–28th August 2014, Lyon*, Elsevier, 2014, pp. 1162–1171.

[10] C. A. F. Silva, L. Manin, R. G. Rinaldi, D. Remond, E. Bbsnier, and M.-A. Andrianoely, "Modeling of power losses in poly-V belt transmissions: hysteresis phenomena (standard analysis)," *J. Adv. Mech. Des. Syst. Manuf.*, vol. 11, no. 6, 2017.

[11] C. A. F. Silva, L. Manin, R. G. Rinaldi, D. Remond, E. Besnier, and M. A. Andrianoely, "Modeling of power losses in poly-V belt transmissions: hysteresis phenomena (enhanced analysis)," *Mech. Mach. Theory*, vol. 121, pp. 373–397, 2018.

[12] R. Komanduri and Z. B. Hou, "Analysis of heat partition and temperature distribution in sliding systems," *Wear*, vol. 251, no. 1–12, pp. 925–938, Oct. 2001.

[13] N. Laraqi, N. Alilat, J. M. G. de Maria, and A. Baïri, "Temperature and division of heat in a pin-on-disc frictional device—Exact analytical solution," *Wear*, vol. 266, no. 7–8, pp. 765–770, Mar. 2009.

[14] A. Yevtushenko, M. Kuciej, and E. Och, "Modeling of the temperature regime and stress state in the thermal sensitive pad-disk brake system," *Adv. Mech. Eng.*, vol. 10, no. 6, p. 168781401878128, 2018.

[15] K. Behdinan and R. Moradi-Dastjerdi, Heat Transfer Behavior of Graphene-Reinforced Nanocomposite Sandwich Cylinders. *Advanced Multifunctional Lightweight Aerostructures: Design, Development, and Implementation*. 2021, pp. 25-42.

[16] Z. Wei, Y. Kan, Y. Zhang, and Y. Chen, "The frictional energy dissipation and interfacial heat conduction in the sliding interface," *AIP Adv.*, vol. 8, no. 11, Nov. 2018.

[17] G. Gerbert, *Force and slip behaviour in V-belt drives*, vol. 67. Helsinki: Finnish Academy of Technical Sciences, 1972.

[18] B. G. Gerbert, *Pressure distribution and belt deformation in V-belt drives*, no. 3. Lund, 1975.

[19] B. Bhushan, *Modern tribology handbook*. Boca Raton: CRC Press, 2001.

[20] B. G. Gerbert, "Some notes on V-Belt drives," *J. Mech. Des. Trans. ASME*, vol. 103, no. 1, pp. 8–18, Jan. 1981.

[21] X. Liu and K. Behdinan, "A novel analytical model for the thermal behavior of a fiber-reinforced plastic pulley in a front-end accessory drive," *Adv. Mech. Eng.*, vol. 12, no. 6, p. 168781402092449, Jun. 2020.

[22] X. Liu and K. Behdinan, "Analytical-Numerical Model for Temperature Prediction of a Serpentine Belt Drive System," *Appl. Sci.*, vol. 10, no. 8, p. 2709, Apr. 2020.

[23] X. Liu and K. Behdinan, Modeling and Experimentation of Temperature Calculations for Betl Drive Transmission Systems in the Aviation Industry. *Advanced Multifunctional Lightweight Aerostructures: Design, Development, and Implementation*. 2021, pp. 123-149.

[24] X. Liu and K. Behdinan, "Innovative Analytical Model for Temperature Prediction of Front-end Accessory Drive," *Sci. Rep.*, vol. 11, no. 1, p. 1476, Jan 2021.